Progress In Electromagnetics Research M, Vol. 27, 41–57, 2012

DETERMINATION OF THE CONVEX HULL OF A RADIATING SYSTEM IN A HETEROGENEOUS BACKGROUND

Amedeo Capozzoli, Giuseppe D'Elia*, and Pietro Vinetti

Dipartimento di Ingegneria Biomedica, Elettronica e Delle Telecomunicazioni, Università Degli Studi di Napoli Federico II, Naples, Italy

Abstract—Recently, referring to a homogeneous background, a new technique estimating the convex hull of a source/scattering system from the radiated/scattered electromagnetic field data has been presented. In this paper, the approach is extended to the inhomogeneous background case by considering the source/scattering system and the observation domain embedded in two different homogeneous media. The underlying theory has been properly reformulated to account for the refraction phenomenon arising at the electromagnetic discontinuities boundaries by considering a 2D geometry. The performances of the technique have been estimated by means of a numerical analysis whose main representative results are presented and discussed in the paper.

1. INTRODUCTION

The determination of the convex hull containing a set of electromagnetic sources/scatterers, the Observed System (OS), later on, from the knowledge of the radiated/scattered field, the observed field (OF) later on, on an observation domain is a problem of relevant interest, both from the theoretical and practical point of view, in the framework of Inverse Source (IS) or Inverse Scattering (ISC) problems.

As a matter of fact, many applications, from the detection of voids and reinforcements in concrete to the detection of mines or underground cavities, involve the solution of ISC problems [1–5].

Basically, the solving approach relies on the optimization of an objective functional, which, in principle, due to the missing of a priori information, should require global optimization procedures to

Received 27 July 2012, Accepted 25 September 2012, Scheduled 13 November 2012

* Corresponding author: Giuseppe D'Elia (g.delia@unina.it).

avoid false solutions corresponding to the trapping into local optima. Unfortunately, global optimization could turn to be unfeasible due to the high computational burden required, and the ill-conditioning that could often affect it [6, 7]. Thus, in almost any practical case, the optimization is performed by exploiting local procedures, which seriously affects the reliability of the solutions.

Obviously, any a-priori information can mitigate the above difficulties, since it can provide a more favorable starting point of the searching. In particular, any information restricting the investigation region allows reducing the occurrence of local minima as well as the computational load [8–10].

The knowledge of the convex hull containing the observed system provides very useful information. Obviously, a convex hull finding technique represents a valuable tool only if it requires a negligible effort, as compared to the one necessary to solve the full inverse problem.

On the other side, as referred above, there are relevant applications wherein the knowledge of the convex hull of an OS is of interest by itself, as, f.i., in the case of mine or concrete voids detection.

However, the convex hull finding technique presented and experimentally verified in [8, 11, 12] has been formulated in the case of homogeneous backgrounds in the sense that both the observed system and the observation line are essentially embedded in the same medium.

The aim of this paper is to generalize the approach to the inhomogeneous case, wherein the observation line and the observed system are embedded in two different homogeneous media with different electromagnetic properties, as depicted in Fig. 1.

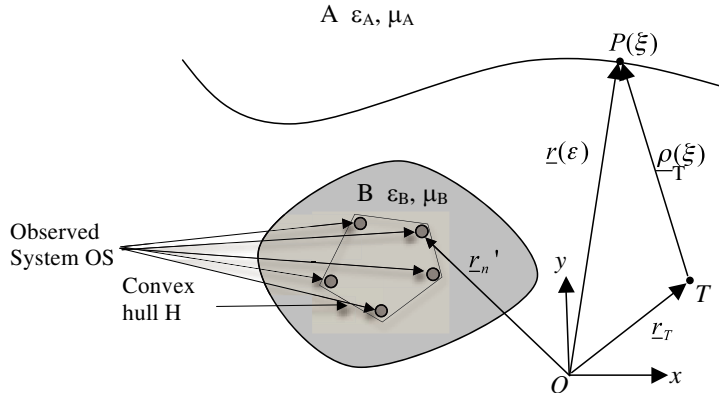

Figure 1. Geometry of the problem: (C) observation curve, (OS) observed system and (H) convex hull.

The paper is organized as follows. The theory underlying the proposed technique and the solution strategy are presented in Section 2, while Section 3 and Section 4 are focused on the case of two geometries of practical interest: a line discontinuity with a line observation domain and a circular discontinuity with a circular observation domain, respectively.

The main representative results of a wide numerical analysis carried out to evaluate the performances of the technique for the two considered geometries are discussed in Section 5.

Conclusions are drawn in Section 6.

2. UNDERLYING THEORY AND SOLUTION STRATEGY

Let us consider the geometry depicted in Fig. 1, relative to a 2D OS analyzed in the case of a scalar, single frequency/single view configuration. The $\exp(j\omega t)$ field time dependence will be omitted later on when writing the expressions for the field.

The background region is characterized by two media, say A and B (white and gray areas in Fig. 1), with electromagnetic parameters and wavelengths, ε_A, μ_A, λ_A and ε_B, μ_B, λ_B, respectively. We assume that medium A contains the observation curve, whose parametric representation is denoted with $P(\xi)$. On the other hand, medium B is assumed to contain OS, composed of N radiators/scatterers whose sizes are assumed to be small or comparable with λ_B and whose spacings are assumed to be larger than $2 \div 3\lambda_B$.

As in [8], the technique here proposed resides on the local properties of the radiated/scattered field [13], which is here applied to the inhomogeneous case.

To this end, let us consider a reference system (O, x, y) and denote with $E(\xi)$ and $E(\xi,\ \underline{r}_n)$ the OF at $P(\xi)$ and the contribution from the n-th radiator/scatterer, respectively. By generalizing [8], let us define the "reduced" field $F_T(\xi)$ with respect to a reference point T as

$$F_T(\xi) = E(\xi) \cdot \exp\{j\beta\rho_T(\xi)\} \tag{1}$$

where $\underline{\rho}_T(\xi) = \underline{r}(\xi) - \underline{r}_T$, $\rho_T(\xi) = \left|\underline{\rho}_T(\xi)\right|$, $\underline{r}(\xi)$ and $\underline{r}_T$ are the position vectors locating the observation and reference points P and T, respectively, and $\beta = 2\pi/\lambda_0$ (no losses are assumed in the media), λ_0 being the wavelength.

The spatial local properties of the field can be analyzed by means of the *sliding window spectrum* [14], i.e., the local Fourier transform of

the reduced field around a point $P(\xi)$:

$$\tilde{F}_T(\kappa,\xi) = \int F_T\left(\xi'\right) g\left(\xi'-\xi\right) \exp\left(-j\kappa\xi'\right) d\xi'$$
$$= \int E\left(\xi'\right) \exp\left[j\beta\rho_T\left(\xi'\right)\right] g\left(\xi'-\xi\right) \exp\left(-j\kappa\xi'\right) d\xi' \quad (2)$$

where $g(\xi)$ is a windowing function and κ is the variable conjugate to ξ.

First, let us consider a point-wise radiator/scatterer, f.i., the n-th component of the OS located at $\underline{r}_n$. By exploiting the *Sommerfeld-Runge* [15] conjecture†, the corresponding electromagnetic field on the observation line, say $E(\xi,\underline{r}_n)$, can be expressed as:

$$E(\xi,\underline{r}_n) = E_0(\xi,\ \underline{r}_n)\exp[-j\beta S(\xi,\underline{r}_n)] \quad (3)$$

where $E_0(\xi,\underline{r}_n)$ and $S(\xi,\underline{r}_n)$ are a complex and a real function, respectively, slowly varying on spatial intervals comparable to λ_0.

From Eq. (2), the sliding window spectrum of the n-th contribute to the reduced OF, say $\tilde{F}_T(\kappa,\xi,\underline{r}_n)$, is given by:

$$\tilde{F}_T(\kappa,\xi,\underline{r}_n) = \int E_0\left(\xi',\underline{r}_n\right) g\left(\xi'-\xi\right) \exp\left[j\psi\left(\xi',\underline{r}_n\right)\right] \exp\left(-j\kappa\xi'\right) d\xi' \quad (4)$$

$$\psi(\xi,\underline{r}_n) = \beta\left[\rho_T(\xi) - S(\xi,\underline{r}_n)\right] \quad (5)$$

Accordingly, in the geometrical optics approximation, i.e., when $\beta \to +\infty$, the integral in Eq. (4) can be asymptotically evaluated by the stationary phase method. Neglecting end points and/or slope contributions, only stationary points, roots of the equation:

$$-\frac{d\psi}{d\xi} + \kappa = 0 \quad (6)$$

give a significant contribution to $\tilde{F}_T(\kappa,\xi,\underline{r}_n)$, provided that they fall inside the sliding window. Therefore, for a given value of the parameter ξ, the sliding window spectrum is significantly different from zero for those values of κ such that:

$$\kappa \approx \frac{d\psi}{d\xi} = h_T(\xi,\underline{r}_n) \quad (7)$$

Hence, the function $h_T(\xi,\underline{r}_n)$ provides the spatial local bandwidth, around the point $P(\xi)$, of the reduced (with respect to T) field radiated by the n-th component of the OS. According to [8, 13], the function $h_T(\xi,\underline{r}_n)$ will be called *Point Source Spectral Content* (PSSC) of the point-wise source/radiator located at $\underline{r}_n$.

† It is assumed that the working conditions are not too far from those of Geometrical Oprtics.

Since each element of the OS contributes to the OF at the point $P(\xi)$, it can be assumed that the spatial *Local (Reduced) Field Bandwidth* (LRFB or simply LFB), say $w_T(\xi)$, of the reduced OF by the whole OS accounts for the contribution (the PSSCs) of each element, each one centered on the relative PSSC, as:

$$w_T(\xi) = \max_{\underline{r}_n} |h_T(\xi, \underline{r}_n)| = \max_{\underline{r}_n} \left| \beta \frac{\partial [\rho_T(\xi) - S(\xi, \underline{r}_n)]}{\partial \xi} \right| \tag{8}$$

It must be noted that such contributions are related to and contains information on the position of each radiator/scatterer. Accordingly, information on these positions, useful to find the convex envelope of the whole OS, could be obtained once the LFB has been properly estimated. However, in principle, since these contributions sum up coherently, an interference effect can occur, in an unpredictable way, making difficult to distinguish each contribution from the estimated LFB [16]. In this case, an incoherent multi-illumination should be exploited as in [16]. In the following, thanks to the assumptions that the radiators/scatterers are not too close each other, the LFB can be correctly estimated from the field data without exploiting the strategy in [16].

It's worth noting that, for a given reference point T, the LFB is a function of ξ only. On the other hand, if the point $P(\xi)$ is fixed while the reference point T is moved along a curve, $w_T(\xi)$ varies due to the hidden dependence of $\rho_T(\xi)$ on T. As shown in [17], the minimum value of $w_T(\xi)$ is attained when the following condition is verified:

$$\frac{d\psi}{d\xi} = \frac{\beta}{2} \left[\max_{\underline{r}_n} \frac{\partial S}{\partial \xi} + \min_{\underline{r}_n} \frac{\partial S}{\partial \xi} \right] \tag{9}$$

The corresponding minimum value of the LFB is given by:

$$\begin{aligned} w_{\min} &= \min_T w_T(\xi) = w_{T^*(\xi)}(\xi) = \frac{\beta}{2} \left[\max_{\underline{r}_n} \frac{\partial S}{\partial \xi} - \min_{\underline{r}_n} \frac{\partial S}{\partial \xi} \right] \\ &= \frac{\beta}{2} \left[\max_{\underline{r}_n} \frac{\partial S}{\partial s} - \min_{\underline{r}_n} \frac{\partial S}{\partial s} \right] \frac{ds}{d\xi} \end{aligned} \tag{10}$$

where s is the curvilinear abscissa on the curve C and $T^*(\xi)$ is the reference point where $w_T(\xi)$ attains its minimum value.

Obviously, these results include also the homogeneous case. In fact, when $\varepsilon_A = \varepsilon_B$ and $\mu_A = \mu_B$ the rays arising from the n-th element propagate unperturbed along straight trajectories and the eikonal function S reduces essentially to the distance: $R(\xi, \underline{r}'_n) = |\underline{r}(\xi) - \underline{r}_n|$, thus obtaining the results provided in [8]. In particular, in [8] $w_{\min}$ is shown to be related to the minimum angular sector under which the OS is "seen" from the point $P(\xi)$.

Similarly, in the next two Sections, it will be shown that in the inhomogeneous case, $w_{\min}$ is related to the closest optical rays from the point P that, after refraction on the boundary discontinuity, fully encloses the OS.

Accordingly, the approach here presented, exploiting Eq. (10), finds the convex hull of the OS by the following steps:

i) The scattered field on the observation line C is acquired;
ii) The line Γ wherein the reference point T will be located is chosen;
iii) For each observation point on the observation line C corresponding to the parameter ξ, the reference point T is moved along Γ; for each position of T, given the OF measured on the observation line, the sliding window spectrum is evaluated and $w_T(\xi)$ estimated. Among all the positions of T, the reference point, say $T^*(\xi)$, corresponding to that providing the minimum value for $w_T(\xi)$ is found together with such a minimum, $w_{T\,\min}(\xi)$ say;
iv) Thanks to the knowledge of both $T^*(\xi)$ and $w_{T\,\min}(\xi)$, the two extreme rays stemming from the point $P(\xi)$ are traced such that, after refraction through the discontinuities, the minimum angular region including the OS is given (see Sections 3 and 4 for the formulas related to the cases of rectilinear and circular lines);
v) Choose another observation point on C and repeat the operations at points iii) and iv);
vi) Estimate the convex hull as the intersection of all the angular regions corresponding to all the considered observation points on C.

The equations required to evaluate the two optical rays stemming from each observation point $P(\xi)$ that, after the refraction through the discontinuities, gives the minimum angular region including the scattering system, depend on C and Γ, and are given in Sections 3 and 4 for the geometries here considered.

3. THE CASE OF A RECTILINEAR DISCONTINUITY AND OBSERVATION CURVE

Let's consider the case of a rectilinear discontinuity, depicted in Fig. 2 with equation $y = y_d$, and a rectilinear observation curve with equation $y = y_{obs}$.

The parameter ξ is now assumed equal to x and the PSSC of the field due to the n-th scatterer can be easily evaluated from (7) putting $\xi = x$ and taking into account that

$$\frac{\partial}{\partial x} |\underline{r} - \underline{r}_T| = \hat{i}_{\rho_T} \cdot \hat{i}_x = \cos[\phi_T(x)] \tag{11}$$

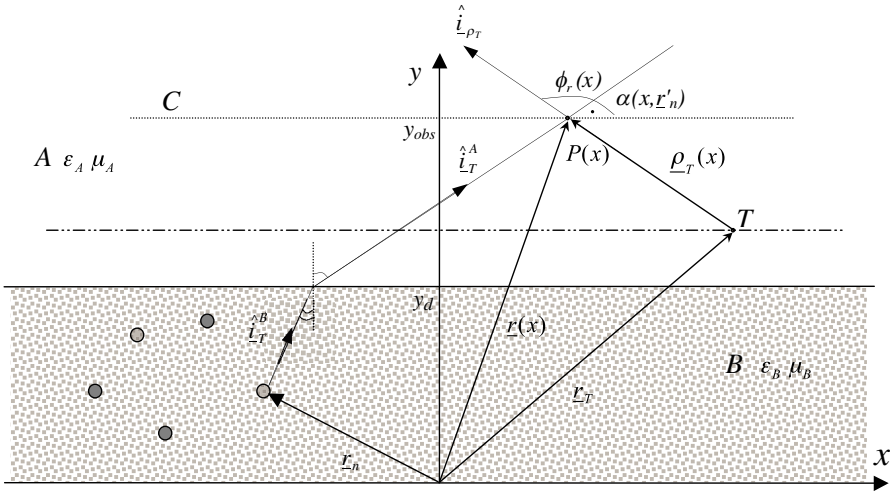

Figure 2. Geometry of the problem in the linear case.

and

$$\frac{\partial S}{\partial x} = \nabla S \cdot \hat{i}_x = n_A \hat{i}_t^A \cdot \hat{i}_x = n_A \cos[\alpha(x, \underline{r}_n)] \tag{12}$$

where $\hat{i}_{\rho T}$ and $\hat{i}_x$ are the unit vectors of the vector $\underline{\rho}_T(x)$ and of the x-axis, respectively, $\phi_T(x)$ is the angle between them, $\hat{i}_t^A$ is the unit vector of the ray stemming, in the medium A, from the n-th scattering element and reaching $P(x)$, and $\alpha(x, \underline{r}'_n)$ is the angle between $\hat{i}_t^A$ and $\hat{i}_x$.

From Eqs. (5), (7), (11) and (12) one obtains:

$$h_T(x, \underline{r}_n) = \beta[\cos\phi_T(x) - n_A \cos\alpha(x, \underline{r}_n)] \tag{13}$$

To find $w_{\min}(x)$ and $T^*(x)$ let us fix $P(x)$ and move the reference point T along a line Γ parallel to the x axis (Fig. 3) so that the second term in the bracket of Eq. (13) varies with T while the first one stays constant. It is noted that Γ could be also a non rectilinear curve, and can also intersect the observed system. As shown in [8], the minimum value for $w_T(x)$ is achieved when:

$$\cos\left[\phi_{T^*(x)}(x)\right] = \frac{1}{2}\left\{\max_{\underline{r}_n}\left[n_A \cos\alpha(x, \underline{r}_n)\right] + \min_{\underline{r}_n}[n_A \cos\alpha(x, \underline{r}_n)]\right\} \tag{14}$$

and is equal to:

$$w_{\min}(x) = w_{T^*(x)}(x) = \frac{\beta}{2}\left\{\max_{\underline{r}_n}[n_A \cos\alpha(x, \underline{r}_n)] - \min_{\underline{r}_n}[n_A \cos\alpha(x, \underline{r}_n)]\right\} \tag{15}$$

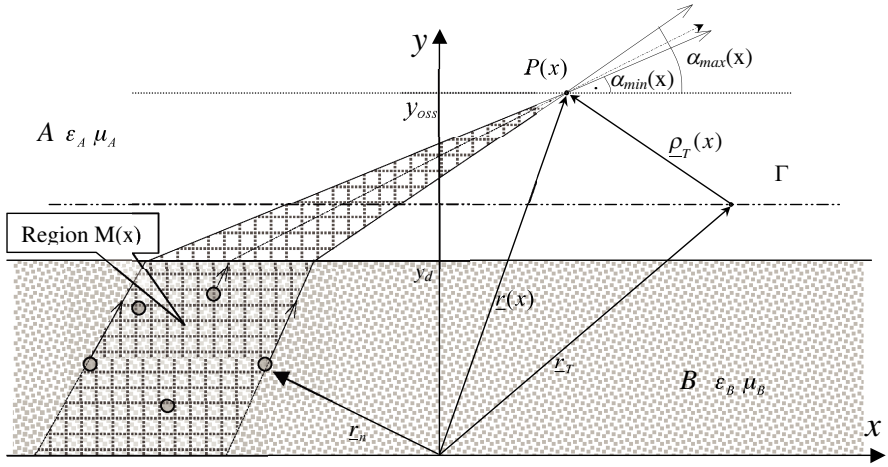

Figure 3. Determination of the angular region $M(x)$.

Accordingly, from the knowledge of $w_{\min}(x)$ and $T^*(x)$ (and, thus $\cos[\phi_{T^*(x)}(x)]$), obtained by suitably processing the OF on the observation line C, the values of $\alpha_{\min}(x)$ and $\alpha_{\max}(x)$ such that:

$$\begin{aligned} \cos\alpha_{\min}(x) &= \max_{\underline{r}_n}\left[\cos\alpha(x,\underline{r}_n)\right] \\ \cos\alpha_{\max}(x) &= \min_{\underline{r}_n}\left[\cos\alpha(x,\underline{r}_n)\right] \end{aligned} \tag{16}$$

can be found from Eqs. (14) and (15).

It is worth noting that $\alpha_{\min}$ and $\alpha_{\max}$ define the two optical rays stemming from $P(x)$ that, after refraction at the discontinuity, give the minimum angular region, say $M(x)$, containing the OS (see Fig. 3).

According to the point vi) in the previous Section, an estimate of the convex hull enclosing the radiating system is achieved by intersecting all the regions $M(x)$ corresponding to all the considered observation points.

Obviously, the choice of the line Γ must ensure the attainment of $w_{\min}(x)$. According to the previous considerations, this is ensured when Γ is long enough and located between the OS and the observation line.

4. THE CASE OF A CIRCULAR OBSERVATION DOMAIN

Let's now consider a different background arrangement, depicted in Fig. 4. B is a circular medium (the grey region in the figure) with

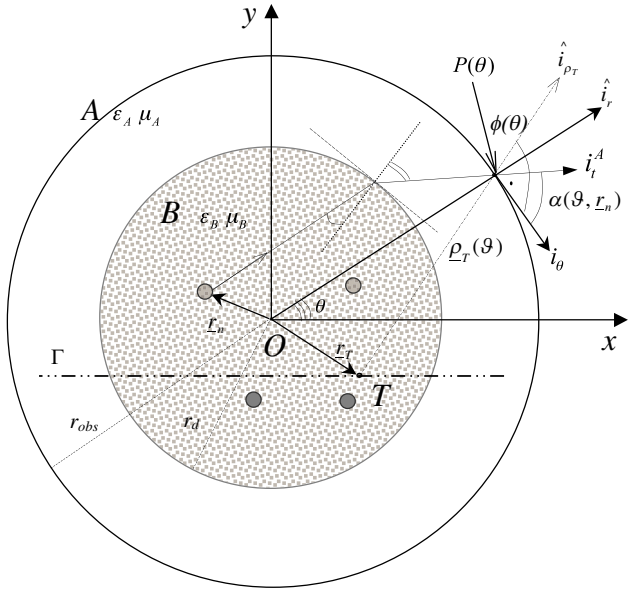

Figure 4. Geometry of the problem in the circular case.

radius r_d, containing the scattering system, and is immersed in the medium A (white in the figure). According to the geometry of the problem, it is convenient to introduce a polar reference system (O, r, θ) centered on the region B, and to chose as observation domain, C, a circumference of radius $r_{obs} > r_d$ concentric with B.

The parameter ξ is now assumed equal to θ, and, from (7), the PSSC of a given elementary source/scatterer is given by:

$$\begin{aligned} h_T(\vartheta, \underline{r}_n) &= \frac{\partial}{\partial \vartheta} \beta \left[|\underline{r}(\vartheta) - \underline{r}_T| - S(\vartheta, \underline{r}_n) \right] \\ &= \beta [\cos(\phi_T(\vartheta)) - n_A \cos(\alpha(\vartheta, \underline{r}_n))] \end{aligned} \tag{17}$$

where $\alpha(\theta, \underline{r}_n)$ is the angle between $\hat{i}_\vartheta$ and $\hat{i}_t^A$ and $\phi(\theta)$ is the angle between and $\hat{i}_{\rho_T}$ and $\hat{i}_\vartheta$, $\hat{i}_\vartheta$ being the unit angular vector, $\hat{i}_{\rho_T}$ the unit vector joining T to $P(\theta)$ and $\hat{i}_t^A$ the unit vector of the optical ray arriving at $P(\theta)$ from the point-wise source/scatterer located at $\underline{r}_n$ (See Fig. 4).

Again, for a given observation point $P(\theta)$, when moving the reference point T along a line Γ, parallel to the x-axis, only the first

term in the bracket of Eq. (17) varies, and it attains its minimum value:

$$w_{\min}(\vartheta) = w_{T^*(\vartheta)}(\vartheta) = \frac{\beta}{2}\left\{\max_{\underline{r}_n}\left[n_A\cos\alpha(\vartheta,\underline{r}_n)\right] - \min_{\underline{r}_n}\left[n_A\cos\alpha(\vartheta,\underline{r}_n)\right]\right\} \quad (18)$$

as long as the reference point T attains the point $T^*(\vartheta)$ such that:

$$\cos[\phi_{T^*(\vartheta)}(\vartheta)] = \frac{1}{2}\left\{\max_{\underline{r}_n}\left[n_A\cos\alpha(\vartheta,\underline{r}_n)\right] + \min_{\underline{r}_n}\left[n_A\cos\alpha(\vartheta,\underline{r}_n)\right]\right\} \quad (19)$$

Therefore, once the point $T^*(\vartheta)$ and the value of $w_{\min}(\vartheta)$ are found from the available OF, the relationships (18) and (19) allow to estimate the value of $\alpha_{\min}$ and $\alpha_{\max}$ as:

$$\begin{aligned}\cos\alpha_{\min}(\vartheta) &= \max_{\underline{r}_n}\left[\cos\alpha(\vartheta,\underline{r}_n)\right]\\ \cos\alpha_{\max}(\vartheta) &= \min_{\underline{r}_n}\left[\cos\alpha(\vartheta,\underline{r}_n)\right]\end{aligned} \quad (20)$$

Obviously, $\alpha_{\min}$ and $\alpha_{\max}$ are related to the region M, introduced in the previous Section (see Fig. 5).

Accordingly, also in this case the estimate of the convex hull is obtained as the intersection of all the regions M's corresponding to all the considered observation points.

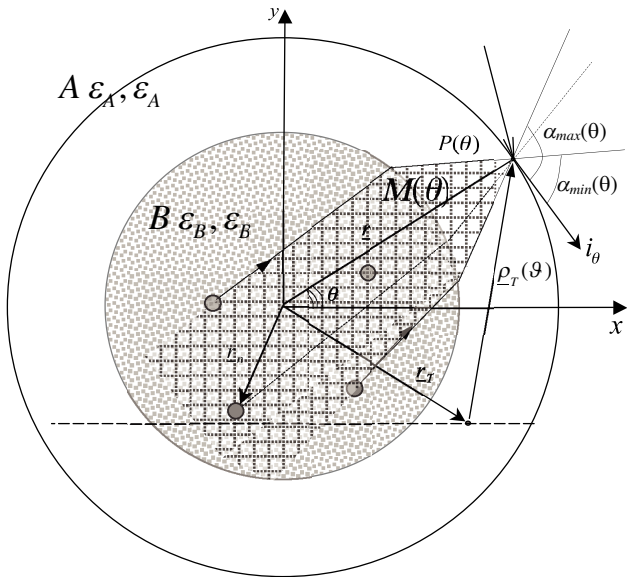

Figure 5. Determination of the angular region $M(\theta)$.

It is worth noting that, at variance of the previous case, now the observation line surrounds the OS, and a better estimate of the convex hull is expected.

5. NUMERICAL RESULTS

The effectiveness of the approach has been checked by simulating numerically the scattered field in a two-dimensional scalar case. The main results of a wide numerical analysis are reported in the following.

In order to estimate the agreement between the reconstructed convex envelope and the exact one, a quality figure, say Q, is considered. Let us denote with E the set of points defining the estimated envelope and by E_0 the exact envelope. We set

$$Q = \frac{\text{Meas}((E \cup E_0))/(E \cap E_0))}{\text{Meas}(E \cup E_0)} \tag{21}$$

where Meas() denotes the measure of the set, while $\cap$ and $\cup$ denote the intersection and the union of two sets, respectively. Q is equal to 0 when the envelope is exactly estimated ($E \equiv E_0$) and to 1 when $E \cap E_0 \equiv \emptyset$, $\emptyset$ being the void set. To show the performance of the technique under different working conditions, the cases of metallic only, or dielectric only scatterers are considered as well as the case of a hybrid set of metallic and dielectric scatterers.

Furthermore, in the case of only dielectric scatterers, two configurations corresponding to different contrasts with respect to the host background are also reported, to show the robustness of the presented technique against such a parameter.

Let us consider first a set of five copper cylindrical scatterers, with a diameter equal to $0.2\lambda_0$, located at $(0, 5\lambda_0)$, $(\lambda_0, 5\lambda_0)$, $(3\lambda_0, 4\lambda_0)$, $(-4\lambda_0, -3\lambda_0)$, and $(2\lambda_0, -4\lambda_0)$, embedded in the circular medium B, with radius $14\lambda_0$ and refractive index $n_b = 2$ and a circular observation domain with radius $20\lambda_0$, concentric to B and immersed in a void space (medium A). The primary source is located outside the scanning domain at $(22\lambda_0, 0)$.

The estimated angular regions $M(\theta)$, corresponding to 24 observation points uniformly distributed on the observation circumference are shown in Fig. 6, and the estimated convex hull, whose shape can be easily appreciated in the figure as the intersection of all the angular regions, has a Q value equal to 0.44.

Then, the case of a set of five dielectric scatterers is considered within the same background system of the previous examples. Two different dielectric configurations are here presented: a low contrast one with scatterers refractive index $n_s = 4$, and a high contrast one

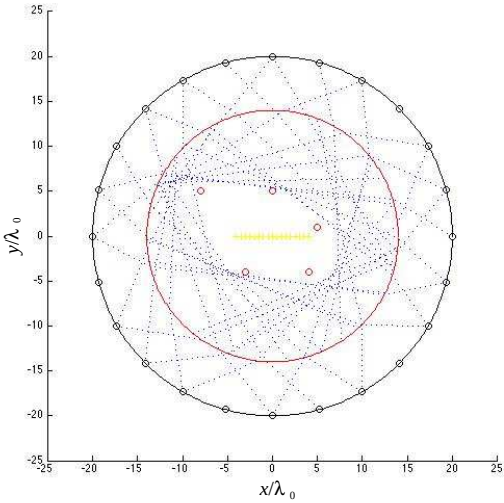

Figure 6. Convex hull estimate: scattering system made of 5 copper elements. Black outer circumference: observation domain; red inner circumference: mediums boundary; blue dashed lines: angular regions; small red circles: copper scatterers.

with scatterers refractive index $n_s = 20$, whose results are reported in Figs. 7(a) and 7(b), respectively. Again, the estimated convex hull can be easily appreciated from the figure as the intersection of all the angular regions. The values of Q are 0.37 and 0.38, respectively. As seen, the algorithm results to be effective also in a case of a dielectric case with a poor contrast.

The case of an heterogeneous scattering system made by three copper cylinders with diameter equal to $0.2\lambda_0$ located at $(-2\lambda_0, 5\lambda_0)$, $(-2\lambda_0, 4\lambda_0)$ and $(5\lambda_0, 2\lambda_0)$ and three dielectric scatterers, with the same diameter and a refractive index $ns = 4$, located at $(-4\lambda_0, 2\lambda_0)$, $(\lambda_0, -5\lambda_0)$ and $(-\lambda_0, 4\lambda_0)$, has been considered, embedded within the same background configuration and with the same source position of the previous examples. The results are shown in Fig. 8(a), and the value of Q is 0.48. As can be seen, a good convex hull estimate is obtained, and the dielectric scatterers does not appear shadowed by the metallic ones.

Then, a completely heterogeneous scattering system is considered with metallic and dielectric scatterers having different electromagnetic permittivity. In particular, two metallic scatterers located at $(-5\lambda_0, -3\lambda_0)$ and $(3\lambda_0, 4\lambda_0)$, and three dielectric scatterers located

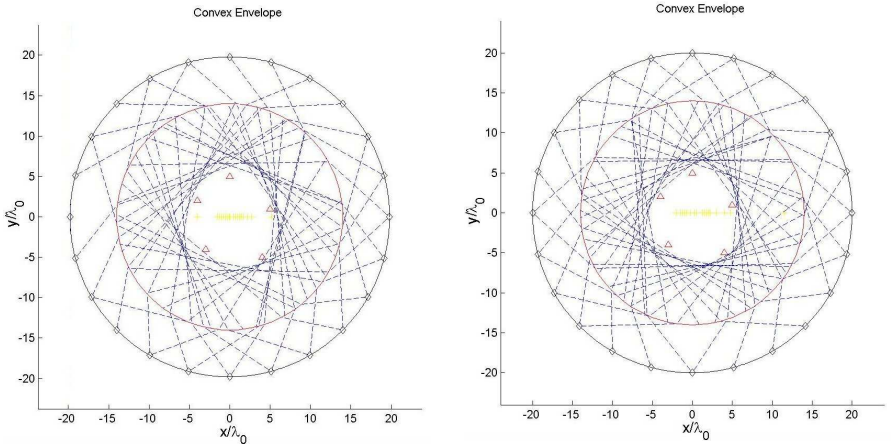

(a) (b)

Figure 7. Convex hull estimate: (a) low contrast dielectric scattering system; (b) high contrast dielectric scattering elements. Black outer circumference: observation domain, red inner circumference: boundary of the inner medium; blue dashed lines: angular regions; small red triangles: dielectric scatterers.

at $(0, 5\lambda_0)$ $(\lambda_0, -6\lambda_0)$ and $(3\lambda_0, -4\lambda_0)$ with refraction index equal to $n_s = 4$, $n_s = 10$ and $n_s = 20$, respectively, are considered. The obtained results are shown in the Fig. 8(b). In this case, Q is equal to 0.46, confirming that, even in this more general case, the presented technique provides a fine convex hull estimation.

Then the case of a rectilinear discontinuity and observation line is analyzed by considering a line discontinuity at $y = 0$, a primary source located at $(0, 10\lambda_0)$, an OS embedded in a medium with refraction index $n_B = 2$, and an observation line in the void with equation $y = 10\lambda$.

In a first case three scattering cylinders with the diameter equal to $0.2\lambda_0$ and located at $(-7\lambda_0, -9\lambda_0)$, $(4\lambda_0, -8\lambda_0)$, and $(3\lambda_0, -16\lambda_0)$ are considered. The first two are made of copper while the last one is dielectric, with refraction index $n_s = 4$. The obtained results are shown in Fig. 9(a).

Then, an OS made of four cylinders with diameter equal to $0.2\lambda_0$ and located at $(5\lambda_0, -14\lambda_0)$, $(-6\lambda_0, -8\lambda_0)$, $(-6\lambda_0, -15\lambda_0)$, and $(4\lambda_0, -5\lambda_0)$, has been considered. The first two are made of copper and the other ones are dielectric, with $n_s = 4$ and $n_s = 12$, respectively. The obtained results are shown in Fig. 9(b).

As seen, the technique provides a good estimate, identifying a

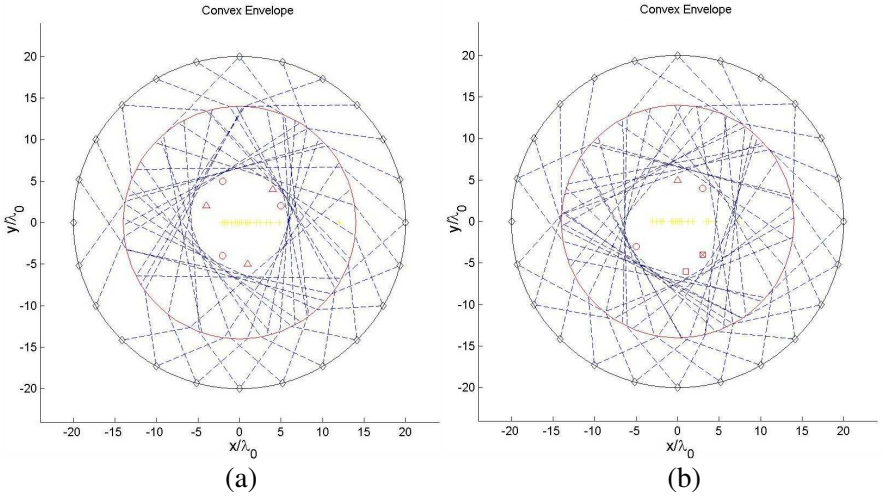

Figure 8. Convex hull estimate: (a) heterogeneous scattering system with copper and identical dielectric elements; (b) heterogeneous scattering system with different dielectric elements. Black outer circumference: observation line; red inner circumference: boundary of the inner medium; blue dashed lines: angular regions; small red circle: copper scatterers; triangle, square, filled square: dielectric scatterers with $ns = 4$, $ns = 10$ and $ns = 20$, respectively.

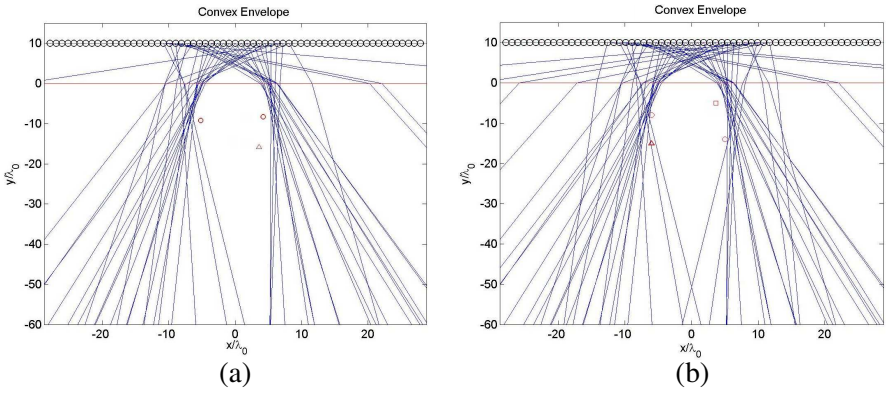

Figure 9. Convex hull estimate: (a) heterogeneous scattering system with identical dielectric elements; (b) heterogeneous scattering system with different dielectric elements. Black line: observation domain; red line: medium boundary, blue lines: angular region; small red circle: copper scatterers; triangles and squares: dielectric scatterers with $ns = 4$ and 10, respectively.

portion of the plane wherein the OS is located. It is worth noting that, although, in principle, a theoretical infinite observation domain should be employed in order to get the actual convex hull, an acquisition domain few tens of wavelengths long is enough to achieve a good estimate of the portion of space containing the observed system. As shown in the figure, this is obtained despite a noticeable lack of accuracy around the dielectric scatterers, especially close to the one with the lower refraction index contrast.

In order to show the effect of noise on the reconstruction algorithm, the case of Fig. 6 has been analyzed by adding a noise to the scattered field. The values of Q, corresponding to a noise on the data (assumed a random, independently and uniformly distributed process) of -20 dB and -30 dB under the field amplitude peak, are 0.59 and 0.51, respectively.

6. CONCLUSIONS

A convex hull finding technique of a radiating/scattering system has been extended to the case of inhomogeneous backgrounds, allowing the technique to be applied to a wider, more interesting, class of problems. Indeed, many practical applications consider OS and observation domains embedded in two different media with different electromagnetic properties.

The performed numerical analysis shows that, despite the approximations of the adopted model, the finding technique provides a good estimate of the convex hull, even when dealing with a complex configuration of scatterers. Furthermore, as required, a relatively small computational burden is needed, as compared to that necessary to solve the full IS or ISC problem.

Accordingly, the proposed technique can be considered as an auxiliary effective tool to be used when solving IS or ISC problems as a pre-conditioner or as a primary tool in all those applications where the convex hull of the scattering system represents the final result.

REFERENCES

1. Kleinman, R. E. and P. M. Van Der Berg, "Two dimensional location and shape reconstruction," *Radio Sci.*, Vol. 29, 1157–1169, Jul.–Aug. 1994.
2. Lesselier, S. D. and B. Duchene, "Wavefield inversion of objects in stratified environments. From backpropagation schemes to full solutions," *Review of Radio Sci. 1993–1996*, W. W. R. Stone, Ed., 235–268, Oxford University Press, 1996.

3. Belkebir, K., R. E. Kleinman, and C. C. Pichot, "Microwave imaging-location and shape reconstruction from multi-frequency scattering data," *IEEE Trans. Microwave Theory Tech.*, Vol. 45, Apr. 1997.
4. Lambert, M., D. Lesselier, and B. J. Kooij, "The retrieval of a buried cylindrical obstacle by a constrained modified gradient method in the H-polarization case and for Maxwellian materials," *Inverse Problems*, Vol. 14, No. 5, 1265–1283, Oct. 1998.
5. Yaman, F., "Location and shape reconstructions of sound-soft obstacles buried in penetrable cylinders," *Inverse Problems*, Vol. 25, No. 6, 065005 + 17, Jun. 2009.
6. Capozzoli, A. and G. D'Elia, "Global optimization and antennas synthesis and diagnosis, Part one: Concepts, tools, strategies and performances," *Progress In Electromagnetics Research*, Vol. 56, 195–232, 2006.
7. Capozzoli, A. and G. D'Elia, "Global optimization and antennas synthesis and diagnosis, Part two: Applications to advanced reflector antennas synthesis and diagnosis techniques," *Progress In Electromagnetics Research*, Vol. 56, 233–261, 2006.
8. Bucci, O. M., A. Capozzoli, and G. D'Elia, "Determination of the convex hull of radiating or scattering systems: A new, simple and effective approach," *Inverse Problems*, Vol. 18, 1621–1638, Dec. 2002.
9. Lencrerot, R., A. Litman, H. Tortel, and J.-M. Geffrin, "Imposing Zernike representation for imaging two-dimensional targets," *Inverse Problems*, Vol. 25, No. 3, 035012 + 18, Mar. 2009.
10. Potthast, R., J. Sylvester, and S. Kusiak, "A range test for determining scatterers with unknown physical properties," *Inverse Problems*, Vol. 19, No. 3, 533–547, Jun. 2003.
11. Bucci, O. M., A. Capozzoll, C. Curcio, and G. D'Elia, "The experimental validation of a technique to find the convex hull of a scattering systems from field data," *IEEE Antennas and Propagation Society International Symposium*, Vol. 1, 539–542, Jun. 22–27, 2003.
12. Capozzoli, A., O. M. Bucci, G. D'Elia, and P. Vinetti, "A new technique finding the convex hull of a scattering system: Performance analysis and application to inhomogeneous backgrounds," *Proc. URSI*, 909–911, May 23–27, 2004.
13. Bucci, O. M., A. Capozzoli, and G. D'Elia, "A novel approach to scatterer localization problem," *IEEE Trans. on Antennas and Propagation*, Vol. 51, No. 8, 2079–2090, Aug. 2003.

14. Daubechies, I., *Ten Lectures on Wavelets*, Society for Industrial and Applied Mathematics, Philadelphia, PA, 1992.
15. Born, M. and E. Wolf, *Principles of Optics*, 7th Edition, Cambridge Press University, Cambridge, UK, 1999.
16. Capozzoli, A., "A novel approach to shape reconstruction from field data," *Atti della XIV Riunione Nazionale di Elettromagnetismo, Atti della XIV RiNEm*, Riunione Nazionale di Elettromagnetismo (RiNEm), Ancona, Italia, Sep. 16–19, 2002.
17. Bucci, O. M., C. Gennarelli, and C. Savarese, "Representation of electromagnetics field over arbitrary surfaces by a finite and non redundant number of samples," *IEEE Trans. on Antennas and Propagation*, Vol. 46, No. 3, Mar. 1998.